Simultaneous Binding of Fluoride and NO to the Nonheme Iron of Photosystem II: Quantitative EPR Evidence for a Weak Exchange Interaction between the Semiquinone Q_A^- and the Iron-Nitrosyl Complex

Yiannis Sanakis,[†] Doros Petasis,[†] Vasili Petrouleas,[‡] and Michael Hendrich*,[†]

Contribution from the Department of Chemistry, Carnegie Mellon University, 4400 Fifth Avenue, Pittsburgh, Pennsylvania 15213, and Institute of Material Science, NCSR "Democritos" 15310 Aghia Paraskevi Attikis, Greece

Received February 19, 1999. Revised Manuscript Received July 19, 1999

Abstract: The effects of NO and fluoride on the iron-quinone complex of the acceptor side of Photosystem II (PSII) are examined by X- and Q-band EPR spectroscopy. It is found that the EPR signal of the iron-nitrosyl complex changes upon addition of F^-. The change is determined to be due to a superhyperfine interaction between the electronic spin ($S = {}^3/_2$) and the fluorine nuclear spin ($I = {}^1/_2$), indicating that both F^- and NO are bound to the same nonheme iron. To the best of our knowledge, this is the first report of simultaneous binding of both F^- and NO to the same iron of a mononuclear nonheme protein. On the basis of an analysis of the hyperfine interaction, a cis F−Fe−NO coordination is indicated. Upon illumination of (NO, Cl^-)- or (NO, F^-)-treated PSII membranes at 200 K, new X- and Q-band EPR signals are observed in $\mathbf{B_1}||\mathbf{B}$ and $\mathbf{B_1}\perp\mathbf{B}$ modes. Quantitative simulations of these signals provide an unambiguous assignment to the iron-quinone complex, $Q_A^-\{FeNO\}^7$ of the acceptor site of PSII. The exchange interaction between the iron-nitrosyl complex ($S = {}^3/_2$) and the semiquinone Q_A^- radical ($S = {}^1/_2$) is determined to be $J = +0.5$ cm^{-1} (F^-) and $+1.3$ cm^{-1} (Cl^-) for $H_{ex} = J\mathbf{S}_1\mathbf{S}_2$. A distribution in the exchange coupling is required to satisfactorily simulate the EPR spectra. This distribution is correlated to small structural variations of the iron-quinone acceptor side of PSII.

The terminal electron acceptor of Photosystem II (PSII)[1] is an iron-quinone complex. On the basis of ample spectroscopic evidence[2] and sequence homologies with the structurally characterized photosynthetic bacteria,[3] it is generally accepted that this complex contains two quinone molecules, Q_A and Q_B, separated by a nonheme iron. The two quinones operate as sequential electron acceptors: Q_A is a one- and Q_B a two-electron acceptor. The iron is coordinated by four histidines, two from each of two subunits. The 5 and 6 coordination positions of the iron differ for bacteria and PSII. In bacteria, these positions are occupied by a bidentate glutamate residue,[3] whereas in PSII at least one of these positions is occupied by bicarbonate.[4] FTIR difference spectroscopy indicates that bicarbonate binds as a bidentate ligand in the Fe^{2+} and a monodentate in the Fe^{3+} state.[4c] Various molecules have been shown to bind in competition with bicarbonate, resulting in reversible deceleration of the electron transfer in PSII.[2]

A direct demonstration of exogenous ligand binding at the iron site of PSII has been provided by treatment with NO.[4a,b] Binding of NO in competition with bicarbonate results in the formation of an $\{FeNO\}^7$ complex ($S = {}^3/_2$) giving rise to a characteristic EPR signal near $g = 4.0$.[5] In addition, cyanide and carboxylates bind at the nonheme iron site in apparent competition with NO or bicarbonate.[6,7] The studies of the effects of the cyanide on the nonheme iron suggest that up to 3 sites at or in the vicinity of the iron are accessible by exogenous ligands.[8] In the present study, we provide unequivocal evidence that both F^- and NO will simultaneously bind to the same iron.

Illumination of PSII at 200 K induces single electron transfer and formation of the $Q_A^-Fe^{2+}$ state at the electron acceptor site. The state has a half-integer spin configuration that gives rise to EPR signals at $g \leq 2.0$. These EPR signals are attributed to a magnetic interaction between Q_A^- and the nearby Fe^{2+} ($S = 2$) ion and are strongly affected by the nature of the labile ligands of the iron.[8,9,10] The analogous signal at $g = 1.82$ in the reaction center of the photosynthetic bacterium *R. Sphaeroides*[11] has been simulated with a weak anisotropic exchange interaction ($J_{iso} \approx$

* To whom correspondence should be addressed. Phone: 412-268-1058. Fax: 412-268-1061. E-mail: hendrich@andrew.cmu.edu.

[†] Carnegie Mellon University.

[‡] Institute of Material Science.

(1) Abbreviations: PSII, Photosystem II; BBY membranes, thylakoid membrane fragments enriched in PSII; DCMU, 3-(3,4-dichlorophenyl)-1,1-dimethylurea; Q_A, Q_B, the primary and secondary plastoquinone electron acceptors of PSII, respectively; EPR, electron paramagnetic resonance; MES, 4-morpholineethanesulfonic acid; Tris, 2-amino-2-hydroxymethylpropane-1,3-diol; EDTA; ethylenediaminetetraacetate.

(2) Diner, B. A.; Babcock, G. T. In *Advances in Photosynthesis: Oxygenic Photosynthesis: The Light Reactions*; Ort, D. R., Yocum, C. F., Eds; Kluwer Academic Publishers: Dordrecht, The Netherlands, 1996; Vol. 4, pp 213−247. (b) Diner, B. A.; Petrouleas, V.; Wendoloski, J. J. *Physiol. Plant* **1991**, *81*, 423−436.

(3) Deisenhofer, J.; Michel, H. *EMBO J.* **1989**, *8*, 2149−2169.

(4) Petrouleas, V.; Diner, B. A. *Biochim. Biophys. Acta* **1990**, *1015*, 131−140. (b) Diner, B. A.; Petrouleas, V. *Biochim. Biophys. Acta* **1990**, *1015*, 141−149. (c) Hienerwadel, R.; Berthomieu, C. *Biochemistry* **1995**, *34*, 16288−16297.

(5) The $\{FeNO\}^7$ nomenclature refers to the covalent FeNO complex which has seven d-electrons.

(6) Deligiannakis, Y.; Petrouleas, V.; Diner, B. A. *Biochim. Biophys. Acta* **1994**, *1188*, 260. (b) Petrouleas, V.; Deligiannakis, Y.; Diner, B. A *Biochim. Biophys. Acta* **1994**, *1188*, 271.

(7) Vermaas, W. F. J.; Rutherford, A. W. *FEBS Lett.* **1984**, *175*, 243.

(8) Koulougliotis, D.; Kostopoulos, T.; Petrouleas, V.; Diner, B. A. *Biochim. Biophys. Acta 1141*, **1993**, 275−282. (b) Sanakis, Y.; Petrouleas, V.; Diner, B. A. *Biochemistry* **1994**, *33*, 9922−9928.

10.1021/ja990533b CCC: $18.00
Published on Web 09/22/1999

0.3 cm^{-1}) between the semiquinone radical ($S = {}^1/_2$) and the high-spin ferrous ion ($S = 2$),[12a] or alternatively by a weaker exchange interaction plus a dipolar term.[12b]

The $g = 4$ EPR signal from the $\{FeNO\}^7$ complex of PSII vanishes upon illumination at 200 K, but photodissociation of NO cannot account for this elimination.[4a,b] Instead, the loss of the $g = 4$ signal has been attributed to the light-induced formation of the state $Q_A^-\{FeNO\}$,[7] which is an overall even electron configuration. No EPR signals attributable to this state have been previously observed. In the present study, we have discovered new signals from the light-induced $Q_A^-\{FeNO\}^7$ state, which establishes the presence of this state and its corresponding electronic properties.

Experimental Methods

PSII-enriched thylakoid membranes were isolated from market spinach by procedures described elsewhere.[13] Some experiments were done in Mn-depleted PSII membranes after treatment with Tris.[14] Samples for EPR measurements were suspended in 0.4 M sucrose, 15 mM NaCl, and 50 mM MES, pH 6.5, at 4−6 mg/mL of chlorophyll. Prior to NO treatment the samples were incubated with variable amounts of NaX (X = Cl, I, Br, F) at 0 °C in the dark. The NO treatment was carried out anaerobically at 0 °C in EPR tubes by slowly bubbling 5 mL of a mixture of NO and N_2 of a given ratio, typically 2/3 or 1/4. This resulted in reproducible concentrations of NO of 0.5−0.7 or 0.1−0.15 mM, respectively, as measured by the characteristic EPR peak of NO in the $g = 2$ region.[4a,b] Illumination of the samples was performed at 200 K in a dry ice/acetone with a 340 W projection lamp filtered through a solution of $CuSO_4$. The samples were then returned to liquid nitrogen temperature prior to spectral measurements.

X-band EPR spectra were recorded on a Bruker spectrometer equipped with an Oxford ESR 910 cryostat for low-temperature measurements and a Bruker bimodal cavity for generation of the microwave fields parallel and transverse to the static field. Q-band EPR spectra were recorded on a Bruker spectrometer equipped with a specially designed low-temperature microwave probe and cryogenic system of our own construction.[15] For both instruments, the microwave frequency was calibrated by a frequency counter and the magnetic field with a gaussmeter. All experimental data were recorded with nonsaturating microwave power unless otherwise noted.

Analysis of Spectra. In this section we collect the relevant terms for the analysis of the spectra. While many parameters are introduced, we will demonstrate that the richness of the spectra allows an unambiguous determination of parameters, first for the $\{FeNO\}^7$ complex and then for the $Q_A^-\{FeNO\}^7$ complex. For the interpretation of the EPR spectra, we use the spin Hamiltonian,

$$H_S = JS_{Fe}S_R + D_{Fe}(S_{z^2} - S(S+1)/3)_{Fe} + E_{Fe}(S_{x^2} - S_{y^2})_{Fe} + \beta B\mathbf{g}_{Fe}S_{Fe} + \beta B\mathbf{g}_R S_R + H_F \quad (1)$$

where J is the isotropic exchange coupling between the iron-nitrosyl and semiquinone radical, D_{Fe} and E_{Fe} are the axial and rhombic zero-field parameters for the iron-nitrosyl site, and g_{Fe} and g_R are the intrinsic g-tensors of the iron-nitrosyl and semiquinone, respectively. The iron-nitrosyl g-tensor may vary from 2 due to second-order spin−orbit interactions. The g-tensor for the quinone is known to be isotropic $g_R = 2$.[8b,16] The last term is the hyperfine contribution from the fluorine nucleus to the iron-nitrosyl site, $H_F = \mathbf{S}_{Fe}\mathbf{A}_F\mathbf{I}_F$, where $\mathbf{A}_F$ is the fluorine hyperfine coupling tensor.

Simulations of the EPR spectra are calculated from diagonalization of eq 1. In dark-adapted samples, the quinone is oxidized ($S_R = 0$) and therefore eq 1 is simplified by the absence of the first and fifth terms. We assume that the weak perturbation of the illumination, which causes the transfer of an electron to the quinone, does not modify the parameters D_{Fe} and E_{Fe}. However, these parameters are modified by binding of the fluorine. The nuclear hyperfine term is treated with second-order perturbation theory. The powder pattern is generated for a uniform spherical distribution of the magnetic field vector **B**. The transition intensities are calculated from Fermi's Golden rule using the eigenfunctions given by the diagonalization. The spectral line shape is generated for distributions of the parameters J and E/D, specified as one standard deviation σ_J and $\sigma_{E/D}$, respectively. A residual line width σ_B in the magnetic field is specified, which is comparable to the magnitude of the magnetic field modulation. Gaussian spin-packets, properly normalized for field-swept spectra,[17] are folded into the spectrum at each resonance field position. Our treatment of the line shape is unique in that it is based on the physical description of the spin system given by eq 1, rather than on the common practice of phenomenological line widths in the magnetic field. Thus, fewer parameters are required and these parameters have physical significance.

The simulations are generated with careful consideration of all intensity factors, both theoretical and instrumental, to allow direct scaling of spectra to sample concentrations. The only unknown variable quantity, relating spin concentration to signal intensity, is an instrumental factor that depends on the microwave detection system. This factor is then determined by a spin standard, CuEDTA, for which the copper concentration was accurately determined from plasma emission spectroscopy.

We present below the predictions of eq 1 in graphic form for the case $J/D < 0.1$, which, as will be shown, applies to the present data. For an $S_{Fe} = {}^3/_2$ site (e.g., $\{FeNO\}^7$) and an $S_R = {}^1/_2$ site (e.g., the semiquinone radical, Q_A^-), and an exchange interaction that is weak relative to the zero-field splitting ($J \ll D$), the lowest four energy levels can be calculated with perturbation theory to obtain analytic expressions for the observed g-values of the transitions as a function of the dimensionless parameter J/f, where f is the microwave frequency. The expressions for the energies of the lowest four levels are derived in Appendix 1. Figure 1 shows a plot of the experimentally observed g-values for magnetic fields along the principal axis directions and for $E/D = 0.020$. This latter value is selected to correspond approximately to the present spectra. Small variations in E/D do not significantly affect the data of Figure 1. This plot provides insight into the interpretation of resonance patterns, which is not always clear from simulations alone. There are three groups of resonances with significant intensity labeled on the plot (I, II, III), with subscripts referring to the principal magnetic field directions. Observed resonance positions can be read off of this plot; for example at X-band (9.5 GHz, 0.317 cm^{-1}) with $J = 0.4$ cm^{-1}, resonances would be observed near $g = 2.5$ (272 mT), 9 (85 mT), and 5 (153 mT) from groups I, II, and III, respectively.

Results

Effects of F^- on the $\{FeNO\}^7$ EPR Signal. PSII membranes previously treated with 25 mM NaCl or NaF in the dark for 1 h were further incubated with NO for 45 min at 0 °C. Figure 2 shows X-band (9 GHz) EPR spectra of the Cl^-(A) and F^-(B) samples. As previously reported in the presence of Cl^-,[4a,b] we observe a nearly axial signal with $g_y = 4.10$ and $g_x = 3.97$

(9) Rutherford, A. W.; Zimmerman, J. L. *Biochim. Biophys. Acta* **1984**, *767*, 168−175. (b) Nugent, J. H. A.; Diner, B. A.; Evans, M. C. W. *FEBS Lett.* **1981**, *124*, 241−244. (c) Nugent, J. H. A.; Doetschman, D. C.; MacLachlan, D. J. *Biochemistry* **1992**, *31*, 2935−2941.

(10) Petrouleas, V.; Sanakis, Y.; Deligiannakis, Y.; Diner, B. A. In *Research in Photosynthesis*; Murata, N., Ed.; Kluwer Academic Publishers: Dordrecht, The Netherlands, 1992, Vol. II, pp 119−122.

(11) Dutton, P. L.; Leigh, J. S.; Reed, E. W. *Biochim. Biophys. Acta* **1973**, *292*, 654−664.

(12) Butler, W. F.; Calvo, R.; Fredkin, D. R.; Isaacson, R. A.; Okamura, M. Y.; Feher, G. *Biophys. J.* **1984**, *45*, 947−973. (b) Dismukes, G. C.; Frank, H. A.; Friesner, R.; Sauer, K. *Biochim. Biophys. Acta* **1984**, *764*, 253−271.

(13) Berthold, D. A.; Babcock, G. T.; Yocum, C. F. *FEBS Lett.* **1981**, *134*, 231−234. (b) Ford, R. C.; Evans, M. C. W. *FEBS Lett.* **1983**, *160*, 159−164.

(14) For a review on the treatments affecting the Mn-complex of PSII, see Debus, R. J. *Biochim. Biophys. Acta* **1992**, *1102*, 269−352.

(15) Petasis, D. T.; Hendrich, M. P. *J. Magn. Reson.* **1999**, *136*, 200−206.

(16) Klimov, V. V.; Dolan, E.; Shaw, E. R.; Ke, B. *Proc. Natl. Acad. Sci. U.S.A.* **1980**, *77*, 7227−7231.

(17) Pilbrow, J. R. *Transition Ion Electron Paramagnetic Resonance*; Clarendon Press: Oxford, U.K., 1990; pp 211−259, 341, 631−638.

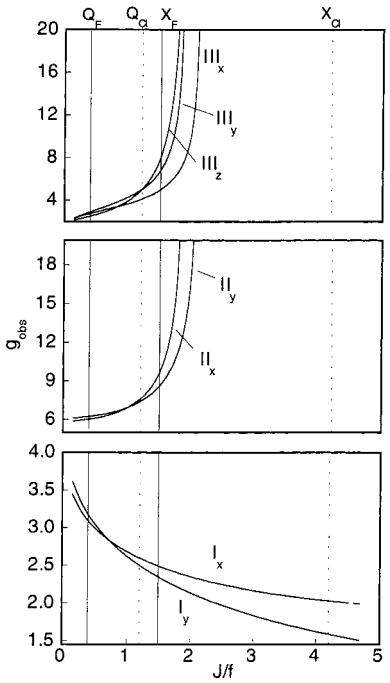

Figure 1. Dependence of the observed **g**-values, $\mathbf{g}_{obs}$, versus J/f for transitions I, II, and III for $E/D = 0.02$. Vertical lines indicate the assignments to the $Q_A^-\{FeNO\}^7$ complex in the presence of F^- (solid line) and Cl^-(dashed line) at X- and Q-band. The subscripts on the transition labels refer to the magnetic field orientation.

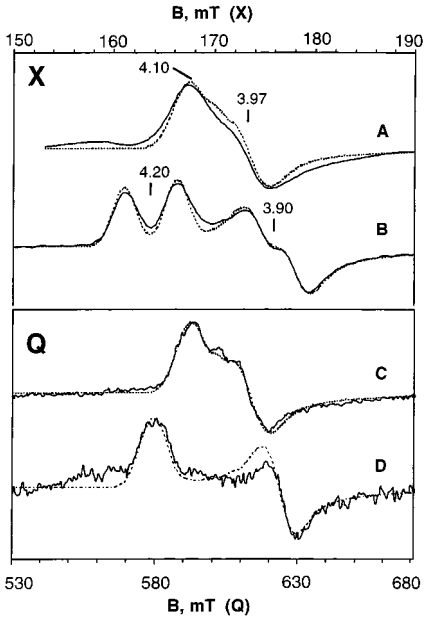

Figure 2. X-band (A, B) and Q-band (C, D) EPR spectra (solid lines) of PSII membranes treated with 25 mM NaCl (A, C) or NaF (B, D) for 1 h at 0 °C in the dark and further incubated with approximately 0.5 mM NO. The simulations (dashed lines) are derived from simultaneous least-squares fits to the X- and Q-band data to an $S_{Fe} = {}^3/_2$ center. For Cl^- (A, C) $D = 10$ cm^{-1}, $E/D = 0.013$, $\sigma_{E/D} = 0.005$, $\mathbf{g} = (2.017, 2.017, 2.000)$. For F^- (B, D) $D = 8$ cm^{-1}, $E/D = 0.026$, $\sigma_{E/D} = 0.004$, $A_x = 101 \pm 5$, $A_y = 146 \pm 5$ MHz, $\mathbf{g} = (2.026, 2.026, 2.000)$. EPR conditions: (A, B) T, 12 K; microwaves, 2 mW at 9.62 GHz; B_{mod}, 12 G_{pp}; (C, D) T, 6 K; microwaves, 0.5 mW at 34.03 GHz; B_{mod}, 5 G_{pp}.

from the $S = {}^3/_2$ FeNO complex.[18] This signal remains unaffected over a broad range of Cl^- concentrations (0.02−100 mM). In the presence of F^-, the signal changes to give two absorption peaks and two derivative features. Figure 2C,D shows Q-band (35 GHz) spectra of the same samples in the presence of Cl^- or F^-, respectively. The spectra are plotted for equal g-value scales at the two frequencies. The Q-band spectrum of the chloride sample is essentially the same, whereas the Q-band spectrum of the fluoride sample collapses to show a typical rhombic species, with g-values of $g_y = 4.20$ and $g_x = 3.90$.

Overlaid on the data of Figure 2 are simulations obtained by simultaneous least-squares fitting of the signals at X- and Q-band to eq 1 using only the iron-nitrosyl terms for $S_{Fe} = {}^3/_2$. The parameters derived for the chloride sample are $E/D = 0.013$, $\sigma_{E/D} = 0.005$, and $\mathbf{g}_{Fe} = (2.017, 2.017, 2.000)$. The line shapes of the spectra are well modeled with a Gaussian distribution in E/D of width $\sigma_{E/D}$. The parameters derived for the fluoride sample are $E/D = 0.025$, $\sigma_{E/D} = 0.004$, and $\mathbf{g}_{Fe} = (2.026, 2.026, 2.000)$. Both the X- and Q-band simulations for the fluoride sample also include an anisotropic superhyperfine interaction to an $I = {}^1/_2$ nucleus of $A_x = 101 \pm 5$ and $A_y = 146 \pm 5$ MHz.[18] From these simulations, the concentration of the iron-nitrosyl complex was found to be 15 μM. The D-value can be determined from the temperature dependence of the intensity of the signals. A fit of the intensity versus temperature to a Boltzmann population of levels (not shown) gave $D = 10 \pm 2$ cm^{-1} in the presence of Cl^- and $D = 8 \pm 2$ cm^{-1} in the presence of F^-. Within the level of uncertainty, we conclude that the effects of F^- on the D-value are minimal., whereas the E/D value in the presence of F^- is significantly larger than the corresponding value in the Cl^- control samples, indicating a higher rhombic distortion for F^-. The splitting of the $g = 4$ signal at X-band in the presence of F^- could possibly be attributed to a superposition of two species with different E/D values. Clearly, however, this is not the case since the spectra at X- and Q-band would then be identical.

The simultaneous match of the simulations to both the X- and Q-band data unequivocally requires a superhyperfine interaction to the $I = {}^1/_2$ ^{19}F nucleus. The magnitude of the A-value indicates that F^- is bound to the FeNO to form an FFeNO complex. To the best of our knowledge, this is the first report of both F^- and NO bound to the same iron of a mononuclear nonheme protein. In the presence of 0.5−0.7 mM NO, the K_d for fluoride binding at the iron-nitrosyl complex was approximately 1 mM. This K_d did not depend on the NaCl concentration, suggesting that Cl^- and F^- do not compete for binding at the iron-nitrosyl complex. We also investigated the effects of other halides on the iron-nitrosyl $g = 4$ signals. Superhyperfine splittings have been observed in EPR spectra of Br ($I = {}^3/_2$) adducts of ferric heme proteins and synthetic analogues.[19a] The $g = 4$ signals obtained in PSII membranes pretreated with 25 mM NaBr or NaI gave signals similar to those of the Cl^- spectrum, suggesting that these ions do not bind at the iron-nitrosyl complex. Furthermore, these results indicate that the fluoride effects are specific and not related to changes in the protein environment in the vicinity of the iron-quinone complex induced by the magnitude of the ionic strength.

Light-Induced Signals from the $Q_A^-\{FeNO\}^7$ Complex. The iron-nitrosyl signal at $g = 4$ is eliminated upon illumination,

(18) The axes x, y, and z are defined by the spin Hamiltonian eq 1, where the largest component of the zero-field splitting tensor is assumed to be along the z-axis. For the $|\pm{}^1/_2>$ state of a $S = {}^3/_2$ system, $g_y > g_x > g_z$. The hyperfine axis system is assumed coincident with the electronic system. The g_z feature near $g = 2$ is obscured by other signals and not shown; thus A_z is also not measurable.

(19) Van Camp, H. L.; Scholes, C. P.; Mulks, C. F.; Caughey, W. S. *J. Am. Chem. Soc.* **1977**, *99*, 8283−8290. (b) Morimoto, H.; Kotani, M. *Biochim. Biophys. Acta* **1966**, *126*, 176−178.

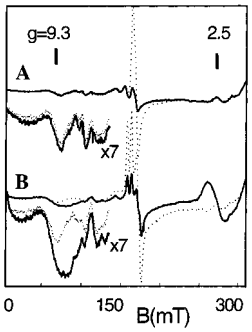

Figure 3. The effect of illumination at 200 K (solid lines) on the X-band EPR spectra of NO-treated PSII membranes in the presence of 25 mM NaCl (A) or NaF (B). The dark spectra (dashed lines) in both samples show weak features in the low-field region which are not light sensitive and are attributed to unidentified impurities. EPR conditions: *T*, 5 K; microwaves, 2 mW at 9.41 GHz; B_{mod}, 25 G_{pp}.

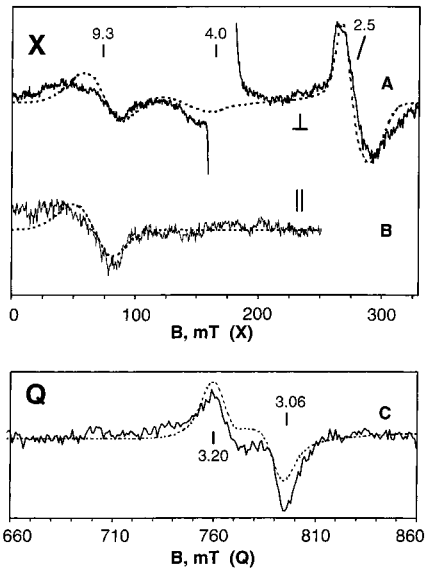

Figure 4. X-band (A, B) and Q-band (C) difference spectra (light minus dark, solid lines) of NO-treated PSII membranes in the presence of 25 mM NaF. Spectrum B is recorded with $\mathbf{B}_1||\mathbf{B}$. The simulations (dashed lines) are derived from simultaneous least-squares fits to the three spectra for an $S_{Fe} = {}^3/_2$ site exchange-coupled to an $S_R = {}^1/_2$ site. The simulation parameters are $D = 8$ cm^{-1}, $E/D = 0.025$, $\sigma E/D = 0.004$, $J = 0.47$ cm^{-1}, $\sigma_J = 0.05$ cm^{-1}, $A_x = 101$, and $A_y = 146$ MHz. EPR conditions are given in Figure 2. The $\mathbf{g} = 4$ signal has been removed for clarity.

but no new EPR signals were observed at X-band.[4a,b] This was believed to be due to a magnetic interaction of {FeNO}^{7} ($S_{Fe} = {}^3/_2$) with the semiquinone Q_A^- ($S_R = {}^1/_2$). Here we present the detection of signals at X- and Q-band that originate from this interaction.

Figure 3 shows X-band EPR spectra before (dashed line) and after (solid line) illumination at 200 K in the presence of Cl^- (A) or F^- (B). Illumination causes a significant decrease in the intensity of the $g = 4$ signals. Illumination induces no new signals in the chloride-treated sample at X-band, while Figure 3B shows new signals appearing at $g = 2.5$ and 9.3 for the fluoride sample. Figure 4A shows the resulting difference spectra for the fluoride sample (light minus dark, solid line). All of the dashed lines in Figure 4 are simulations, which are discussed below. A new light-induced signal also appears near $g = 9$ in the fluoride sample for microwave fields, $\mathbf{B}_1$, oscillating parallel to the applied field **B**. The difference spectrum is shown in Figure 4B. Finally, a new light-induced signal is also observed

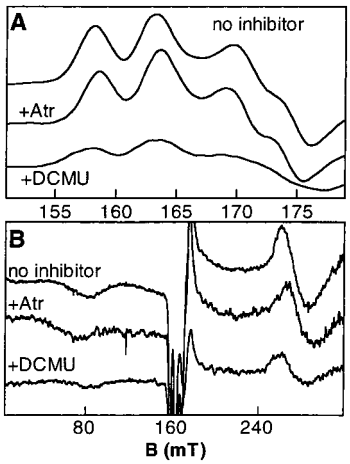

Figure 5. Difference spectra showing the effect of the PSII inhibitors Atrazine and DCMU (100 μM) on the $\mathbf{g} = 4$ iron-nitrosyl signals and the light-induced signals in the presence of 25 mM NaF: (A) dark-illuminated at 200 K, and (B) illuminated at 200 K-dark. EPR conditions: *T*, 5 K; microwaves, 2 mW at 9.41 GHz; B_{mod}, 25 G_{pp}.

at Q-band near $g = 3.1$ in the fluoride sample. Figure 4C shows the difference spectrum at Q-band. The light-induced signals have frequency-dependent *g*-values; thus the X- and Q-band of data Figure 4 are not plotted on an equal *g*-value scale.

A number of control experiments were performed to determine the composition of the species giving the light-induced signals. The light-induced signals are invariably observed in untreated samples or Tris-treated BBY samples which lack the Mn oxygen-evolving cluster. These preparations also show weak EPR signals at $g = 2.95$ and 2.25 from cytochrome b_{559}.[20] No modification of these signals occurs, indicating that cytochrome b_{559} is not responsible for the light-induced signals.

The inhibitors DCMU or Atrazine bind at the Q_B site and are known to affect the signals associated with the iron-quinone complex[7,21] as well as the redox and binding properties of the nonheme iron. In the presence of 0.25 mM NO, the addition of 0.1 mM DCMU reduces the {FeNO}^{7} signal by approximately 50%, while similar concentrations of Atrazine slightly change the rhombicity of the signal, as shown in Figure 5A.[22] Thus, Atrazine perturbs the electronic structure of the iron-nitrosyl without affecting the binding of NO, whereas DCMU raises K_d for NO binding. The light-induced signals in the presence of either of these inhibitors show analogous effects. For Atrazine, the light-induced signal, Figure 5B, retains intensity but small shifts occur. The signal at $g = 9.3$ shifts to lower fields by 100 G, while the signal at $g = 2.5$ shifts to higher fields by 40 G. For DCMU, the light-induced signals are approximately 50% weaker than without DCMU. These observations support the assignment of the light induced signals to the iron-nitrosyl complex.

For samples in the presence of Cl^-, no new X-band EPR signals are observed in either parallel or perpendicular modes upon illumination. However at Q-band, a new signal is observed at $g = 2.6$ and the difference spectrum (light minus dark, solid line) is shown in Figure 6. We will demonstrate below that the lack of a signal at X-band and the presence of signals at Q-band are due to the larger magnitude of the exchange interaction in the presence of Cl^-.

(20) For a review on usual EPR signals from PSII, see Miller, A.-F.; Brudvig, G. W. *Biochim. Biophys. Acta* **1991**, *1056*, 1−8.

(21) Diner, B. A.; Petrouleas, V. *Biochim. Biophys. Acta* **1987**, *893*, 138−148.

(22) D. Koulougliotis, Diploma Thesis, NCSR Democritos, unpublished results.

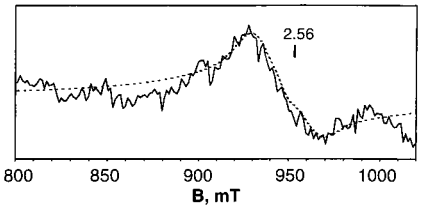

Figure 6. Q-band difference spectrum (light minus dark, solid line) of NO-treated PSII membranes in the presence of 25 mM NaCl. The simulation (dashed line) is derived from a least-squares fit to an $S_{Fe} = {}^3/_2$ site exchange-coupled to an $S_R = {}^1/_2$ site. The simulation parameters are $D = 10$ cm^{-1}, $E/D = 0.013$, $\sigma_{E/D} = 0.005$, $J = 1.32$ cm^{-1}, $\sigma_J = 0.35$ cm^{-1}. The simulation includes a dipolar interaction for $r = 7.0$ Å and $\theta_r = 45°$ (see text). EPR conditions are given in Figure 2.

Assignment of Light-Induced Signals from Samples with Fluoride. We will first consider the signals from the fluoride samples because the spectra are better resolved and observed at both X- and Q-band. Figure 4 shows difference spectra (light minus dark, solid lines) of the FFeNO sample at X-band (parallel and perpendicular modes) and Q-band. Clearly, we must consider that the new light-induced signals may involve the iron-nitrosyl complex, since the $g = 4$ signal from that site vanishes upon illumination. The inhibitor experiments shown above also support this assignment. In addition, many studies have shown that a semiquinone radical, Q_A^-, species is formed in PSII upon illumination at cryogenic temperatures. On the basis of these facts, we consider an exchange coupling between a structurally unmodified iron-nitrosyl ($S_{Fe} = {}^3/_2$) and a semiquinone, Q_A^- ($S_R = {}^1/_2$). The iron-nitrosyl site parameters are derived prior to illumination, and inspection of eq 1 indicates that the only unknown parameter is the exchange coupling parameter, J.

The simulations overlaid on the data of Figure 4 (dashed lines) use the FFeNO site parameters given in Figure 2 prior to illumination. We now vary only the isotropic exchange parameter J and the width σ_J of a distribution in J. We find, for $J = 0.47$ cm^{-1} and $\sigma_J = 0.05$ cm^{-1}, a simultaneous match to all three spectra of Figure 4. There are no adjustable parameters between any of these spectra, and in particular, this also applies to the intensity factors. The simulations are truly quantitative and allow determination of the spin concentration. To within 10%, we find a quantitative conversion of the photosensitive fraction of the $g = 4$ signal of Figure 3 to the light-induced signals of Figure 4. The quantitative simultaneous match to all three spectra allows an unambiguous assignment of these signals to an $S_{Fe} = {}^3/_2$ FFeNO species exchange coupled to the $S_R = {}^1/_2$ semiquinone radical.

A significant distribution in J of 10% is required to match the substantial broadening of the transitions. Such a distribution was considered also in the simulation of the EPR signal from the state $Q_A^-Fe^{2+}$ in the photosynthetic bacterium *R. sphaeroides*.[12a] The position and broadening of the signals can be understood from inspection of Figure 1. For $J = 0.47$ cm^{-1}, transition I gives rise to the derivative signals near $g = 2.5$ (X-band) and $g \sim 3.1$ (Q-band). Transitions II and III_z give the rather weak signals at $g > 8$ (X-band). The broadening is profound for transitions III_x and III_y, which give a weak broad absorption for $4 < g < 8$. The dramatic effect on the line shapes upon inclusion of a distribution of the J-value is due to the dependence of the g_{obs} on J/f in Figure 1. For $1.25 < J/f < 1.56$, the value of g_{obs} for transition I varies by only 4% over this range, while g_{obs} for the other transitions varies by 20−45%. Thus, the effect of a distribution, σ_J, on the broadening of the EPR signals is significantly larger for the transitions II and III than for I. Transition II is not observed in Q-band. This is mainly due to a 12-fold decrease in the transition probability from X to Q-band and partly due to the broadening of the transitions.

We have also considered the following alternative broadening mechanisms, but they all gave unsatisfactory simulations in the absence of a distribution in the J-value. (1) A distribution in E/D. This parameter, although necessary for simulations of the $g = 4$ signals in the dark, had an insignificant effect on the simulation of the light-induced signals. (2) The superhyperfine tensor A of ^{19}F. The splitting due to ^{19}F binding is not resolved, as it is wholly within the line width of the observed signals. (3) Anisotropic exchange interaction. Anisotropic interactions can have pronounced effects on the spectra, but these effects contribute to rather small shifts in the signals that do not properly broaden the spectra. Nevertheless, we have investigated the effect of this interaction in detail.

The most plausible origin for anisotropy in the present case is the dipolar interaction. The dipolar interaction[17] is defined with the vector **r**, joining the two paramagnetic species, and polar angles θ_r and φ_r, which describe the orientation of **r** relative to the **g**-tensor of the $S_{Fe} = {}^3/_2$ spin system. From the crystal structure of the bacterial reaction center, the distance between the iron and the center of the quinone ring is 8.5 Å.[23] We have included the dipolar term into the spin Hamiltonian of eq 1 and into the simulations for **r** in the range 7−10 Å and arbitrary polar angles. While for certain dipolar distances and angles we observe shifts in the simulations, within experimental accuracy, we are not able to detect a significant contribution from a dipolar interaction in the spectral data for the F^- case. This can be rationalized by an appropriate choice of distance and angle that minimizes the dipolar interaction. For example, for $\mathbf{r} = 8.5$ Å, $\theta_\mathbf{r} = 90°$, and $\varphi_\mathbf{r} = 55°$, the simulations give good fits similar to those shown in Figure 4. For $\mathbf{r} \geq 10$ Å, no significant changes are observed in the simulations for any dipolar angles.

Assignment of the Light-Induced Signals from Samples with Chloride. Figure 6 shows the difference spectrum (light minus dark, solid line) of the FeNO sample at Q-band. Again, we consider an exchange coupling between a structurally unmodified iron-nitrosyl ($S_{Fe} = {}^3/_2$) and a semiquinone, Q_A^- ($S_R = {}^1/_2$). The simulation overlaid on the data (dashed line) uses the parameters derived for the FeNO site given in Figure 2 prior to illumination. In addition, the simulation of Figure 6 includes an isotropic exchange interaction of $J = 1.3$ cm^{-1} and $\sigma_J = 0.3$ cm^{-1}. The signal-to-noise of the spectrum is relatively poor due to complications from overlapping signals that do not subtract out well. Nevertheless, the simulations indicate a quantitative conversion of the photosensitive fraction of the $g = 4$ signal in Figure 3 to the light-induced signal of Figure 6. The quantitative agreement allows an assignment of this signal to an $S_{Fe} = {}^3/_2\{FeNO\}^7$ species exchange coupled to the $S_R = {}^1/_2$ semiquinone radical. These signals arise from transition I. The inability to detect signals at X-band can be understood from Figure 1. For $J/f = 4.2$, the only transitions occur at $g = 1.93$ (I_x) and 1.65 (I_y). Simulations (not shown) indicate that the corresponding signals for these transitions are overwhelmed by much stronger signals from other paramagnetic species in this region. At Q-band, transitions II and III are exceedingly broad due to the distribution in J and are therefore difficult to detect.

In contrast to the F^- case, the best simulations of the signal in the presence of Cl^- occur with inclusion of a dipolar

(23) Allen, J. P.; Feher, G.; Yeates T. O.; Komiya, H.; Rees, D. C. *Proc. Natl. Acad. Sci. U.S.A.* **1988**, *85*, 8487−8491. (b) El-Kabbani, O.; Chang, C.-H.; Tiede, D.; Norris J.; Schiffer, M. *Biochemistry* **1991**, *30*, 5361−5369. (c) Emler, U.; Fritzsch, G.; Buchanan, S. K.; Michel, H. *Structure* **1994**, *2* 925−936.

interaction. The dipolar parameters cannot be unambiguously determined as the effects in the spectrum due to this interaction are too subtle. Nevertheless, the simulations are consistent with a distance r in the range 7−9 Å and $\theta_r > 30°$. The simulation shown in Figure 6 is calculated for $r = 7.0$ Å, $\theta_r = 45°$, and $\varphi_r = 0°$.

Discussion

Fluoride Binding at the Nonheme Iron. Fluoride is an inhibitor of O_2 evolution by PSII.[24] Its sites of action appear to be multiple. Apart from the effects of F^- on the donor site of PSII,[14,25] binding at a site sensitive to bicarbonate has been proposed.[26] No spectroscopic evidence has been published so far for fluoride binding at the iron-quinone complex, the main site of action of bicarbonate.[2] Preliminary investigations with variable fluoride concentrations indicated no detectable changes in the EPR signals of the $Q_A^-Fe^{2+}(S = 2)$ and $Fe^{3+}(S = {}^5/_2)$ states. Thus, in the absence of NO, either F^- does not bind at the iron or its binding does not induce detectable effects. However, notable effects are observed on the EPR signals upon F^- addition to the iron-nitrosyl complex.

NO was shown in previous work to bind at the nonheme iron in competition with bicarbonate.[4a,b] In the presence of F^- ($K_d \sim 1$ mM at 0 °C), the EPR signals at $g = 4$ from the $\{FeNO\}^7$ complex of the acceptor site of PSII are significantly modified. The spectra and simulations shown here unambiguously establish that both F^- and NO are bound to the same iron, providing the first direct evidence that the iron has at least two labile ligand positions. Binding of F^- induces a strong superhyperfine interaction of the electron spin with the ^{19}F nucleus. This binding results in small but detectable changes in the zero-field parameters of the iron-nitrosyl complex: an increase in E/D from 0.013 to 0.025 and perhaps a small decrease in D. As mentioned in the Introduction, indirect evidence for multiple Fe coordination sites was observed earlier in the cyanide-binding experiments.[8]

We will consider the structure of the iron environment in the photosynthetic bacteria as a basis for the description of the binding of F and NO at the nonheme iron. The crystallographic data from *R. viridis* and *R. Sphaeroides* show that the nonheme iron resides in a distorted octahedral environment formed by four N_ϵ coordinated His residues: M217 (M219 in *R. Sphaeroides*), L190, L230, and M264 (M266 in *R. Sphaeroides*) and two oxygen donors from Glu M232 (M234 in *R. Sphaeroides*) residue.[3,23] The oxygen ligands and the N_ϵ atoms from His M219 and L190 form an approximate plane, $N_1N_2O_2O_1$ (Figure 7), which contains the iron atom. His M219 interacts with Q_A and His L190 with Q_B. We assume that this geometry can be applied in the nonheme iron of PSII with the difference that the carboxylic oxygen atoms of Glu are now replaced by bicarbonate and in some cases a water ligand. The simplest assumption would be that fluoride and NO substitute for the two oxygen ligands as shown in Figure 7B. The $S = {}^3/_2$ state in octahedral iron-nitrosyl complexes is believed to originate from strong antiferromagnetic coupling between an $Fe^{3+}(S = {}^5/_2)$ and a $NO^-(S = 1)$ species,[27] and the unpaired electrons are predominately found in $d_{x^2-y^2}$, d_{xy}, and d_{z^2} iron orbitals, where the z-axis is along the Fe−NO bond. The $S = {}^3/_2$ state has also been observed in a 5-coordinate trigonal bipyramidal Fe−NO complex.[28] The relatively small change in E/D and D upon binding of fluoride indicates that this FeNO orbital scheme remains applicable. The aforementioned geometric model for PSII suggests that F^- binds cis with respect to NO. Hence, the $d_{x^2-y^2}$, d_{xy} orbitals are presumed to be involved in the fluoride binding. The position trans to NO is then occupied by N from histidine.

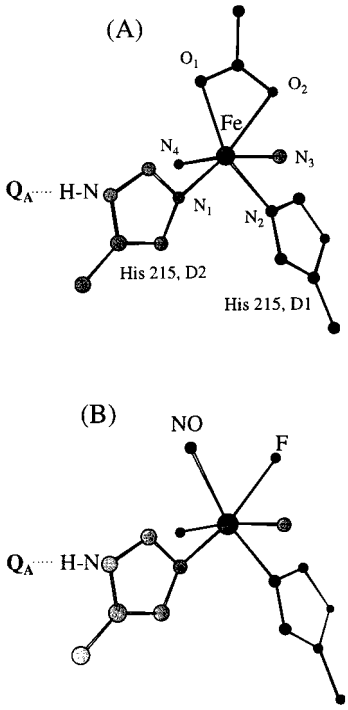

Figure 7. Proposed structure of the nonheme iron environment of PSII in the presence of bicarbonate (bidentate ligand to the iron) (A) or F^- and NO (B). The imidazole rings from the His D2 215 and D1 215, which are believed to interact with Q_A and Q_B, respectively, are included. These residues are homologous to His M219 and L190 of the reaction centers from *R. viridis* (see text). For the "axial" His residues D2 269 and D1 272, only the N_ϵ atoms (N_3, N_4) are shown.

This structural model is supported by an analysis of the superhyperfine tensor components. The binding of fluoride with superhyperfine effects in the EPR spectra is observed for the first time in the nitrosyl complexes of nonheme iron proteins.[29,30] There are many examples of fluoride adducts of heme proteins and synthetic analogues.[19] In all of these cases, the $g_\perp \sim 6.0$ and $g_{||} \sim 2$ EPR signals from the $Fe^{3+}(S = {}^5/_2)$ show splitting due to the superhyperfine interaction with the ^{19}F nucleus. The superhyperfine tensor is axial with $A_x = A_y = 20-22$ G (60 MHz) and $A_z = 43$ G (120 MHz) and collinear with the **g**-tensor. An analysis of the **A**-tensor components in the present case

(24) DeRose, V. J.; Latimer, M. J.; Zimmermann, J.-L.; Mikerji, I.; Yachandra, V. K.; Sauer, K.; Klein, M. P. *Chem. Phys.* **1995**, *194*, 443−459.

(25) Britt, R. D. In *Advances in Photosynthesis: Oxygenic Photosynthesis: The Light Reactions*; Ort, D. R., Yocum, C. F., Eds; Kluwer Academic Publishers: Dordrecht, The Netherlands, 1996; Vol. 4, pp 113−136. (b) Lindberg K.; Andreasson L.-E. *Biochemistry* **1996**, *35*, 14259−14267.

(26) Stemler, A.; Murphy, J. *Plant Physiol.* **1985**, 77, 974−977.

(27) Brown, C. A.; Pavlosky, M. A.; Westre, T. E.; Zhang, Y.; Hedman, B.; Hodgson, K. O.; Solomon, E. I. *J. Am. Chem. Soc.* **1995**, *117*, 715−732.

(28) Ray, M.; Golombek, A. P.; Hendrich, M. P.; Yap, G. P.; Liable-Sands, L. M.; Rheingold, A. L.; Borovik, A. S. *Inorg. Chem.* **1999**, *38*, 3110−3115.

(29) In the NO adduct of the diiron nonheme iron protein deoxyhemerythrin, binding of fluoride was shown to affect the $S = {}^1/_2$ EPR signals arising from the exchange coupling between the Fe_1−NO adduct ($S_1 = {}^3/_2$) with the $Fe_2(S_2 = 2)$. Simultaneous binding of NO and F^- at Fe_1 suggesting a 7-coordinated iron ion was considered unlikely.

(30) Nocek, J. M.; Kurtz, D. M., Jr.; Sage, J. T.; Xia, Y.-M.; Debrunner, P.; Shiemke, A. K.; Sanders-Loehr, J.; Loehr, T. M. *Biochemistry* **1988**, *27*, 1014−1024.

provides information on the nature of the Fe−F bond. A trans or cis coordination of F^- and NO gives different results concerning the expected **A**-tensor as shown below.

I. Fluorine Binds trans to NO. In this case fluorine forms a σ bond through the 2s and $2p_z$ orbitals of fluorine with the d_{z^2} orbital of iron. The resulting molecular orbital is then of the form, $\varphi_{dz^2} = A(d_{z^2}) + B(2s) + C(2p_z)$. The expected hyperfine tensor from the above orbital has the following components:[31]

$$A_x = A_y = (f_{\sigma s}a_s - f_{\sigma p}a_p - A_d)/2S \qquad (2)$$
$$A_z = (f_{\sigma s}a_s + 2f_{\sigma p}a_p + 2A_d)/2S$$

where $a_s = (16\pi/3)g_N\beta\beta_N|\psi(0)|^2$ and $a_p = (^4/_5)g_N\beta\beta_N\langle r^{-3}\rangle$. For ^{19}F, $a_s = +47910$ MHz and $a_p = +1515$ MHz.[32] The parameters $f_{\sigma s}$ and $f_{\sigma p}$ represent the fraction of the unpaired electron found in the 2s and $2p_y$ orbitals, respectively. A_d is the dipolar interaction between the magnetic moment of the central ion and the magnetic moment of the ligand nucleus and is given by the relationship $A_D = 2\ g_N\beta\beta_N r^{-3}$. This case gives an axial **A**-tensor ($A_x = A_y$), which disagrees with the observed *A*-values; thus a trans F−Fe−NO complex is not supported.

II. Fluorine Binds in the *xy*-Plane. In this case fluorine forms σ and π bonds with the d_{z^2}, $d_{x^2-y^2}$, and d_{xy} orbitals. For a fluorine atom on the *y*-axis, the unpaired electrons are found in the following molecular orbitals:

$$\varphi_{d_{x^2-y^2}} = A_1(d_{x^2-y^2}) + B_1(2s) + C_1(2p_y)$$
$$\varphi_{dz^2} = A_2(d_{z^2}) + B_2(2s) + C_2(2p_y) \qquad (3)$$
$$\varphi_{dxy} = A_3(d_{xy}) + B_3(2p_x)$$

The expected hyperfine tensor components from this configuration are the following:

$$A_x = (f_{\sigma s}a_s + (2f_\pi - f_{\sigma p})a_p - A_d)/2S$$
$$A_y = (f_{\sigma s}a_s + (2f_{\sigma p} - f_\pi)a_p - 2A_d)/2S \qquad (4)$$
$$A_z = (f_{\sigma s}a_s + (-f_\pi - f_{\sigma p})a_p - A_d)/2S$$

The parameter f_π represents the fraction of the unpaired electron found in the π orbitals. Here A_x and A_y may be different, in support of fluoride binding in the *xy*-plane, cis to NO in a FFeNO complex. The principal axes of the **A**- and $\mathbf{g}_{eff}$-tensors may not be collinear. While A_z is expected to be parallel to g_z, the principal axes of the **A**- and $\mathbf{g}_{eff}$-tensors in the *xy*-plane may not necessarily coincide. Thus, we have generated simulations for the spectra of Figure 2 with a relative rotation angle, α, between the **g**- and **A**-tensors in the *xy*-plane.[33] As α increases from zero, A_x becomes smaller and A_y larger. For $\alpha = 0°$ or 90°, the difference $|A_y - A_x|$ and the quantity $|f_{\sigma p} - f_\pi|$ take their smallest value and their largest values at $\alpha = 45°$. For an Fe−F bond distance of 2 Å (giving $A_d = 15$ MHz) and $\alpha = 0°$, we find $|f_{\sigma p} - f_\pi| = 6.1\%$, which is comparable to the value found for the myoglobin fluoride adduct of 4.1%.[19b] Since a relative rotation of **A**- and $\mathbf{g}_{eff}$-tensors leads to much larger values for the quantity $|f_{\sigma p} - f_\pi|$, we suggest that either the **A**- and $\mathbf{g}_{eff}$-tensors are collinear (to within ±20°) or the **A**-tensor is rotated 90° (±20°) with respect to the $\mathbf{g}_{eff}$-tensor in the *xy*-plane. For $f_\pi > f_{\sigma p}$, g_x is along the Fe−F bond, whereas for $f_\pi < f_{\sigma p}$, g_y is along the Fe−F bond. In all of the Fe−F complexes studied thus far, the σ-bond is stronger than the π-bond.[19,31,34] Although there is no direct evidence from our experiments that this is the case for the FFeNO complex of PSII, extension of the argument would place g_y along the Fe−F bond.

As mentioned above, we cannot measure the value of A_z, and thus, a direct determination of the isotropic part of the fluorine hyperfine tensor is not possible. However, from eqs 4, we can estimate the maximum isotropic value by noting that f_π, $f_{\sigma s}$, and $f_{\sigma p}$ must all be positive quantities. This requires that A_x, $A_y > 0$, $-248 < A_z < +55$ MHz and therefore the isotropic component is $A_{iso} \leq 100$ MHz, which gives $f_{\sigma s} \leq 0.63\%$. For myoglobin fluoride, this value was found to be 0.82%. The ranges for $f_{\sigma p}$ and f_π are 6.1−26.1% and 0−20%, respectively.

This analysis gives a hint as to the hyperfine splitting expected for other ligands, presumably N and/or O, sharing common orbitals with F in iron-nitrosyl complexes. Although the fraction of unpaired electron spin on $^{14/15}N(I = 1, {}^1/_2)$ or $^{17}O(I = {}^5/_2)$ ligands is likely to be larger than that found in fluorine if electronegativity is considered, the significantly smaller value of a_s and a_p for these elements would be consistent with unresolved hyperfine or minimal broadening in EPR signals.[35]

The Light-Induced Signals from the Q_A^-FeNO Complex. Illumination at low temperatures of untreated PSII membranes induces the state $Q_A^-Fe^{2+}$. Due to the magnetic interaction with the spin ($S = 2$) of the iron, the signal of the semiquinone radical ($S = {}^1/_2$) is broad, and depending on the coordination of the iron, a variety of EPR signals are obtained at $g \leq 2$.[8,9,10] In all of these cases, the number of unpaired electrons in the complex is odd. The $Q_A^-\{FeNO\}^7$ complex has an even number of unpaired electrons. Thus, the light-induced sensitivity of the $g = 4$ signals and the absence of alternative signals has been attributed to EPR silence at X-band due to the even number of unpaired electrons. We have now identified EPR signals with and without fluorine that unequivocally originate from the $Q_A^-\{FeNO\}^7$ spin-coupled system.

In the following, we comment on EPR characteristics which may be applicable to other proteins containing an $S_1 = {}^3/_2$ metal center interacting with an $S_2 = {}^1/_2$ radical or nearly isotropic metal center. For example, similar signals have been observed from the aldehyde ferredoxin oxidoreductase of *Pyrococcus furiosus* and attributed to a weak interaction between a $[Fe_4S_4]^{1+}$ cluster ($S = {}^3/_2$) and a tungsten center ($S = {}^1/_2$).[36] The ratio J/D dictates the behavior of the EPR spectra. For $J/D < 0.01$, the EPR signal from the radical species is broadened. The metal signal extends over several hundred Gauss and is not appreciably affected.[37] For J/D in the range 0.01−0.1, the case encountered in this study, the observed EPR signals deviate significantly from the uncoupled signals. A similar approach was used to describe the weak exchange interaction between $S_{Fe} = {}^5/_2$ and

(31) Owen, J.; Thornley, J. H. M. *Rep. Prog. Phys.* **1966**, *29*, 675−728. (b) Abragam, A.; Bleaney, B. *Electron Paramagnetic Resonance of Transition Ions*; Clarendon Press: Oxford, U.K., 1970.

(32) Wertz, J. E.; Bolton, J. R. *Electron Spin Resonance*; Chapman and Hall, New York, 1986, p 498.

(33) Hoffman, B. M.; Martinsen, J.; Venters, R. A. *J. Magn. Res.* **1984**, *58*, 110−123.

(34) Hall, T. P. P.; Hayes, W.; Stevenson, R. W. H.; Wilkens, J. *J. Chem. Phys.* **1963**, *38*, 1977−1984. (b) Radnell, C. J.; Pilbrow, J. R.; Subramanian S.; Rogers, M. T. *J. Chem. Phys.* **1975**, *12*, 4948−4952.

(35) Arciero, D. M.; Orville, A. M.; Lipscomb, J. D. *J. Biol. Chem.* **1985**, *260*, 14035−14044. (b) Orville, A. M.; Lipscomb, J. D. *J. Biol. Chem.* **1993**, *268*, 8596−8607.

(36) Koehler, B. P.; Mukund, S.; Conover, R. C.; Dhawan, I. K.; Roy, R.; Adams, M. W. W.; Johnson, M. K. *J. Am. Chem. Soc.* **1996**, *118*, 12391−12405.

(37) Examples for weakly interacting $S_1 = {}^3/_2$ and $S_2 = {}^1/_2$ species can be found in Kundalika, M. M.; Eaton, G. R.; Eaton, S. S. *Inorg. Chem.* **1986**, *25*, 2638−2646.

$S_{Cu} = {}^1/_2$ species.[38] In general, EPR signals at low fields are expected for both $\mathbf{B_1}||\mathbf{B}$ and $\mathbf{B_1}\perp\mathbf{B}$. The line shape for the signals with $\mathbf{B_1}||\mathbf{B}$ is reminiscent of integer-spin signals from isolated metal centers,[39] but unlike the normal integer-spin signals, their intensity does not significantly increase in parallel mode as can be deduced from the character of the states involved in these transitions. EPR signals at higher fields are expected for $\mathbf{B_1}\perp\mathbf{B}$, the stronger of which are characterized by *g*-values near 2.5. As *J*/*D* increases, the low-field signals move toward lower fields, while the high-field signals move toward higher field values, as shown in Figure 1. When *J*/*D* exceeds a characteristic threshold, no signals are observed. This threshold is smaller for the low-field transitions and depends on the microwave energy. Thus, we observe signals at X- and Q-band from the Q_A^-{FeNO}^{7} complex of PSII in the presence of fluoride, but only at Q-band without fluoride. As *J*/*D* further increases, the expressions derived from the perturbation approximation are no longer valid. The case for $J/D > 1$ has been discussed elsewhere.[40]

The shifts of the light-induced signals in the presence of Atrazine can be explained by a slightly larger value of $J = 0.51$ cm^{-1}. Spectral simulations (not shown) indicate that a change in *E*/*D* cannot account for this observed modification of the light-induced signal. Inspection of Figure 1 shows that, upon increase of *J*, the g_{obs}-value decreases for transition I and increases for transitions II and III_z, which is observed in the signal shifts with Atrazine.

A proper description of the exchange interaction requires knowledge of the structure of the Q_A^-{FeNO}^{7} complex and the associated orbital scheme. Currently, we can only make general remarks based on the assumed similarities between PSII and the photosynthetic bacteria. For the bacterial complex, the through bond, metal-quinone exchange interaction consists of an imidazole linkage of the intervening His residue (M219 in *R. sphaeroides*, M217 in *R. viridis*, D2 215 in PSII), which provides the N_ϵ atom as a ligand to the metal[41] as diagrammed in Figure 7. X-ray crystallographic data suggest that the N_δ of the His M219 and the oxygen of Q_A are within a hydrogen-bond distance.[42] The existence of this hydrogen bond has been supported by spectroscopic studies.[43] ESEEM and FTIR studies[44a−d] of PSII also suggest the presence of a hydrogen bond between Q_A and the His 215 of the D2 protein; however, alternative interpretations of the ESEEM spectra have been suggested.[44e] While no detailed description exists, a hydrogen bond may provide a pathway for the exchange interaction between Q_A^- and the metal site in PSII. For the iron-nitrosyl complex, we find that binding of F^- decreases the exchange interaction. This can be rationalized by either an elongation of the distance between the paramagnetic species[45] or an electronic rearrangement of the iron-nitrosyl complex. The lower exchange interaction may also decrease the electron-transfer rate between Q_A and Q_B, but other factors may overwhelm this effect, such as proton transfer and electronic rearrangements.

The line shape and the relative intensity of the transitions in all of the recorded spectra were reproduced assuming a distribution in *J* of 10% in the F^--treated samples and 20% in the Cl^- sample. We would like to comment on the implications imposed by the values of the distribution on *J*. Often *J* and the distance between spin centers, *r*, are correlated with the empirical relationship $J(r) = J_0\exp(-r/r_0)$.[45] The decrease in the *J* observed in the F^- sample is then attributed to an increase in *r*.[46] This elongation, however, cannot be arbitrarily large. A large distance implies a decrease in the His-semiquinone interaction resulting possibly in the loss of any magnetic interaction if the hydrogen bond is the pathway for the exchange interaction. Two representative values are $r \sim 7$ Å in the Cl^- case and $r \sim 8$ Å for the F^- case. With *J* known for the two cases, we find that $J_0 = 1600$ cm^{-1} and $r_0 = 0.98$ Å. From these values, the distribution of *J* of 20% observed in the Cl^- sample will occur for a distribution in r of 0.2 Å. In the F^- sample, the smaller value of σ_J can be attributed to a distribution in *r* of 0.1 Å. Incorporation of a "$J - r$" strain effect is also found in the literature.[47] We do not claim that this is an accurate model for taking into account the uncertainties discussed above; however, it illustrates that a relatively large distribution in *J* does not necessarily imply an unreasonable large structural heterogeneity.

In conclusion, we have presented the first direct evidence for the simultaneous binding of both F^- and NO to the same iron of a mononuclear nonheme protein. The fluorine hyperfine analysis supports a cis F−Fe−NO complex. Upon illumination, new EPR signals are detected with and without fluoride and quantitatively assigned to an exchange interaction between Q_A^- and the {FeNO}^{7} complex. The presence of fluoride decreases the exchange interaction. A distribution in the exchange coupling is required to satisfactorily simulate the EPR spectra, indicating small structural variations of the iron-quinone acceptor side of PSII.

Appendix

We consider an exchange interaction between the an $S_1 = S_{Fe} = {}^3/_2$ site and an $S_2 = S_R = {}^1/_2$ site. For an exchange interaction, which is weak relative to the zero-field splitting ($J \ll D$), the lowest four energy levels can be treated with perturbation theory. The ground doublet of the $S_1 = {}^3/_2$ site can be described by the eigenfunctions $|\pm\tilde{}^1/_2\rangle = c_1|{}^3/_2,\pm{}^1/_2\rangle + c_2|{}^3/_2,\mp{}^3/_2\rangle$ where c_1 and c_2 are functions of *E*/*D*:[17]

(38) Ogasenyan, V. S.; Butler, C. S.; Watmough, N. J.; Greenwood, C.; Thomson, A. J.; Cheesman, M. R. *J. Am. Chem. Soc.* **1998**, *120*, 4232−4233.

(39) Hendrich, M. P.; Debrunner, P. G. *Biophys. J.* **1989**, *56*, 489−506.

(40) Euler, W. B. *Inorg. Chem.* **1986**, *25*, 1871−1875.

(41) Calvo, R.; Passeggi, M. C. G.; Isaacson, R. A.; Okamura, M. Y.; Feher, G. *Biophys. J.* **1990** *58*, 149−165.

(42) Allen, J. P.; Feher, G.; Yeates T. O.; Komiya, H.; Rees, D. C. *Proc. Natl. Acad. Sci. U.S.A.* **1988**, *85*, 8487−8491. (b) El-Kabbani, O.; Chang, C.-H.; Tiede, D.; Norris J.; Schiffer, M. *Biochemistry* **1991**, *30*, 5361−5369. (c) Emler, U.; Fritzsch, G.; Buchanan, S. K.; Michel, H. *Structure* **1994**, *2*, 925−936.

(43) Bosch, M. K.; Gast, P.; Hoff., A. J.; Spoyalov, A. P.; Tsvetkov, Y. D. *Chem. Phys. Lett.* **1995**, *239*, 306−312.

(44) Astashkin, A. V.; Kawamori, A.; Kodera, Y.; Kuroiwa, S.; Akabori, K. *J. Chem. Phys.* **1995**, *102*, 5583. (b) Deligiannakis, Y.; Jegerschold, C.; Rutherford, A. W. *Chem. Phys. Lett.* **1997**, *270*, 564−572. (c) Astashkin, A. V.; Hara, H.; Kuroiwa, S.; Kawamori, A.; Akabori. K. *J. Chem. Phys.* **1998**, *108*, 10143−10151. (d) Noguchi, T.; Inoue, Y.; Tang, X.-S. *Biochemistry* **1999**, *38*, 399−403 (e) Peloquin, J. M.; Tang, X.-S.; Diner, B. A.; Britt, R. D. *Biochemistry* **1999**, *38*, 2057−2067.

(45) Coffmann, R. E.; Buettner, G. R. *J. Phys. Chem.* **1979**, *83*, 2387−2392.

(46) An increase in *r* could be inferred by dipolar parameters. Unfortunately, in the F^- case the dipolar contribution does not appear to be significant. If we assume that the angle between *r* and the **g**-tensor from the Cl^- to the F^- sample is retained, then we must increase the distance in order to eliminate the dipolar effects.

(47) Guigliarelli, B.; Guillaussier, J.; More, C.; Setif, P.; Bottin; H.; Bertrand, P. *J. Biol. Chem.* **1993**, *268*, 900−908, (b) Bertrand, P.; More, C.; Guigliarelli, B.; Fournel, A.; Bennett, B.; Howes, B. *J. Am. Chem. Soc.* **1994**, *116*, 3078−3086.

(48) Analogous theoretical treatment has been carried out for the excited, $|\tilde{}^3/_2\rangle$ state. We find that either no transitions can be induced between the energy levels or the transition probabilities are negligible.

$$c_1 = \frac{-1 - \sqrt{1 + 3(E/D)^2}}{\sqrt{2}\sqrt{1 + 3(E/D)^2 + \sqrt{1 + 3(E/D)^2}}}$$

$$c_2 = \frac{\sqrt{3}(E/D)}{\sqrt{2}\sqrt{1 + 3(E/D)^2 + \sqrt{1 + 3(E/D)^2}}} \qquad \text{(A1)}$$

For the matrix representation of the perturbation Hamiltonian $J\mathbf{S}_1\mathbf{S}_2$, the basis states are $|m_1 = \pm\,{}^1/_2,\ m_2 = \pm\,{}^1/_2\rangle$. In zero magnetic field, diagonalization of the 4×4 matrix results in four energy levels with eigenvalues and eigenfunctions quoted in Table 1. It is useful to express the resulting eigenstates in the coupled $|S,M\rangle$ rather than in the $|M_1,M_2\rangle$ representation, where S is the total spin ($S = 1, 2$), M is the quantum number corresponding to S_z, and M_1, M_2 refer to S_{1z}, S_{2z}. The energies are a linear function of J, while the dependence on c_1 and c_2 (i.e., on E/D) is more complicated. The main observation is that, for appropriate values of J, the separation of the levels is such that EPR transitions can be observed upon application of a magnetic field.

The dependence of the energy levels on B oriented parallel to the three principal axes for constant J and $E/D = 0.02$ are given in eqs A2−5 and plotted in Figure 8.

a. B||x.

$$E_i = \underset{1,3}{\overset{2,4}{\pm}} \frac{\sqrt{3}c_1c_2 + c_1^2}{2} J \underset{1,2}{\overset{3,4}{\pm}} \frac{1}{2}\sqrt{4\left(\frac{1}{2} \underset{1,3}{\overset{2,4}{\pm}} c_1^2 \underset{1,3}{\overset{2,4}{\pm}} \sqrt{3}c_1c_2\right)^2 (g\beta B)^2 + \left(mc_1^2 - \sqrt{3}c_1c_2 \underset{1,3}{\overset{2,4}{\pm}} \frac{3}{2}\right)^2 J^2} \qquad \text{(A2)}$$

$m = 3, -1$ for levels 1,3 and 2,4 respectively.

b. B||y.

$$E_i = \underset{1,2}{\overset{3,4}{\pm}} \frac{c_1^2 - \sqrt{3}c_1c_2}{2} J \underset{1,3}{\overset{2,4}{\pm}} \frac{1}{2}\sqrt{4\left(c_1^2 - \sqrt{3}c_1c_2 \underset{1,2}{\overset{3,4}{\pm}} \frac{1}{2}\right)^2 (g\beta B)^2 + \left(mc_1^2 \underset{3,4}{\overset{1,2}{\pm}} \sqrt{3}c_1c_2 - \frac{3}{2}\right)^2 J^2} \qquad \text{(A3)}$$

$m = 3, 1$ for levels 1,2 and 3,4 respectively.

c. B||z.

$$E_{1,4} = \left[-c_1^2 + \frac{3}{4}\right] \mathrm{J} \underset{1}{\overset{4}{\pm}} Jc_1^2\left[1 + 4\left(\frac{c_2}{c_1}\right)^4 \left(\frac{g\beta B}{\mathrm{J}}\right)^2\right]^{1/2} \qquad \text{(A4)}$$

$$E_{2,3} = \left[c_1^2 - \frac{3}{4}\right] J \underset{3}{\overset{2}{\pm}} [3c_1^2 c_2^2 \mathrm{J}^2 + (c_1^2 - c_2^2)^2 (g\beta B)^2]^{1/2} \qquad \text{(A5)}$$

The eigenstates are not quoted. EPR transitions for both $\mathbf{B}_1||\mathbf{B}$ and $\mathbf{B}_1\perp\mathbf{B}$ can be observed between the various levels if the resonance condition, $\Delta E = h\nu$, is fulfilled and the transition probability is reasonably large. To facilitate the analysis, we have grouped the transitions in three categories I, II, and III and label them according to the corresponding axis.[48]

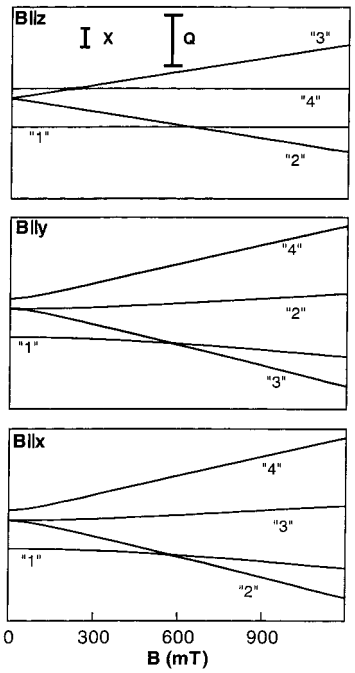

Figure 8. Dependence of the lowest four energy levels on the magnetic field for B||x,y,z and $D = 10$ cm^{-1}, $E/D = 0.02$, and $J = 0.4$ cm^{-1}. The labeling of the levels corresponds to the ordering in energy at zero field (Table 1). The vertical bars indicate the microwave energy at X- and Q-band.

B||*x,y,z*; Transitions between Levels 2 and 3. When **B**||*x,y* the Zeeman term mixes the zero-field states (Table 1) allowing for transitions between levels 2 and 3 (transitions I_x, I_y) in perpendicular mode. For **B**||*z*, mixing between the zero-field states does not occur and perpendicular transitions are forbidden. Transitions for $\mathbf{B}_1||\mathbf{B}$ are observed provided that the transition probability is reasonably large. For two states $|a\rangle$ and $|b\rangle$ that have the property $S_z|a\rangle = |b\rangle$ and $S_z|b\rangle = |a\rangle$, the transition probability varies as $(\Delta/h\nu)^2$, where Δ is the absolute value of the separation of the levels in zero field. For the levels 2 and 3, $\Delta = |\sqrt{3}c_1c_2J|$. The dependence of c_2 on E/D (eq A1) indicates that the transition probability is negligible for $E/D < 0.1$ and becomes significant only as E/D approaches its maximum at ${}^1/_3$. The transition probability also depends on frequency and decreases as the microwave frequency increases.

B||*x*, "Levels 2−4"; B||*y*, "Levels 3−4". The eigenstates are a mixture of the zero-field states (Table 1). Transition set II are observed for $\mathbf{B}_1||\mathbf{B}$ from these levels. The separation of the levels at zero field is $\Delta_x = |(c_1^2 + \sqrt{3}c_1c_2 - {}^3/_2)J|$ for II_x and $\Delta_y = |(c_1^2 - \sqrt{3}c_1c_2 - {}^3/_2)J|$ for II_y. A transition with intensity $\sim(\Delta/h\nu)^2$ may be observed if either Δ_x or Δ_y is less than $h\nu = 0.31$ cm^{-1} (X-band), which is the case for $J < 0.62$ cm^{-1} and $E/D = 0$.

Table 1. The Four Lowest Lying States of an $S_1 = {}^3/_2$ Site Weakly Exchange Coupled to an $S_2 = {}^1/_2$ site ($J \ll D$) at Zero Magnetic Field

energy	state
$(-2c_1^2 + {}^3/_4)J$	$c_1\|1,0\rangle + c_2/\sqrt{2}\,(\|2,-2\rangle - \|2,+2\rangle)$
$(c_1^2 + \sqrt{3}c_1c_2 - {}^3/_4)J$	$\left({}^1/_2\sqrt{\frac{3}{2}}c_1 + \frac{\sqrt{2}}{4}c_2\right)(\|2,+1\rangle - \|2,-1\rangle) - \left(\frac{\sqrt{2}}{4}c_1 - {}^1/_2\sqrt{\frac{3}{2}}c_2\right)(\|1,+1\rangle + \|1,-1\rangle)$
$(c_1^2 - \sqrt{3}c_1c_2 - {}^3/_4)J$	$\left({}^1/_2\sqrt{\frac{3}{2}}c_1 + \frac{\sqrt{2}}{4}c_2\right)(\|2,+1\rangle + \|2,-1\rangle) - \left(\frac{\sqrt{2}}{4}c_1 - {}^1/_2\sqrt{\frac{3}{2}}c_2\right)(\|1,+1\rangle - \|1,-1\rangle)$
${}^3/_4J$	$c_1\|2,0\rangle + c_2/\sqrt{2}\,(\|2,-2\rangle + \|2,+2\rangle)$

B||*x*, "Levels 3−4"; B||*y*, "Levels 2−4"; B||*z*, "Levels 2−4". These transitions have nonzero transition probability in perpendicular mode and, as for transitions II, are observed provided that $J < 0.62$ cm^{-1} for $E/D = 0$.

All transitions have significant intensity, but a distribution in J causes substantial broadening of the signals. This broadening is greatest for transitions II and III; thus transition I is easier to detect from relatively heterogeneous protein solutions.

Acknowledgment. This work was supported by NIH GM49970 (M.P.H.) and the Greek Secretariat of Research and Technology (grant PENED 1139) (V.P.). Y.S. is indebted to Prof. Eckard Münck for support (NIH grant GM22701) and comments concerning the manuscript. The authors wish to thank Dr Y. Deligiannakis for helpful discussions, Dr N. Ioannidis for assistance in the preparation of PSII samples.

JA990533B